Available online at www.sciencedirect.com
SCIENCE DIRECT
Journal of Catalysis 238 (2006) 88–99
JOURNAL OF CATALYSIS
www.elsevier.com/locate/jcat

Thermally stable trivalent iron-substituted hexagonal mesoporous aluminophosphate (FeHMA) molecular sieves: Synthesis, characterization, and catalytic properties

P. Selvam *, S.K. Mohapatra

Solid State and Catalysis Laboratory, Department of Chemistry, Indian Institute of Technology-Bombay, Powai, Mumbai 400076, India

Received 2 June 2005; revised 23 November 2005; accepted 4 December 2005

Available online 9 January 2006

Dedicated to Professor Hemant V. Keer on the occasion of his 70th birthday.

Abstract

Thermally stable trivalent iron-substituted hexagonal mesoporous aluminophosphate (FeHMA) molecular sieves were synthesized and systematically characterized using analytical and spectroscopic techniques, including XRD, TEM, ICP–AES, TGA–DTA, N_2 sorption, DRUV–vis, EPR, and Mössbauer spectroscopy. The characterization studies showed that framework substitution of trivalent iron in tetrahedral framework position of the mesoporous aluminophosphate has taken place. Mössbauer revealed the presence of a small amount of divalent iron. This material has high thermal stability with regard to the dislodgement of trivalent iron from the framework structure on calcination and showed excellent activity in the liquid-phase oxidation of cycloalkanes such as cyclohexane, cyclooctane, and cyclododecane in presence of molecular oxygen or air under mild reaction conditions. FeHMA behave as a heterogeneous catalyst; the catalytic activity was practically unaffected by recycling experiments. Furthermore, the oxidation was successful for the bulkier cycloalkane molecules. A comparative study with selected iron-containing molecular sieve-based catalysts indicated that FeHMA is a promising heterogeneous catalyst with respect to its microporous analogue (FeAPO-5) as well as the silicate analogues, microporous FeS-1 and mesoporous FeMCM-41.

Keywords: Mesoporous; Aluminophosphates; Iron; FeHMA; Oxidation; Cycloalkanes; Cyclohexane; Cyclooctane; Cyclododecane

1. Introduction

The importance of trivalent iron complexes in biological oxidation as well as their use as catalysts in conjunction with a variety of oxidants in organic synthesis has prompted extensive studies under homogeneous reaction conditions [1–8]. However, these homogeneous catalyst systems are often impracticable because of easy deactivation, difficulties in regeneration, and separation of the catalyst. This has led to the development of cleaner, environmentally benign heterogeneous catalytic routes, which may replace conventional stoichiometric or homogeneously catalyzed organic synthesis. Over the years, various supported catalysts have been suggested for this purpose; however, the leaching of active metal ions resulted in a short catalyst lifetime [9]. Trivalent iron-substituted molecular sieves (silicates, aluminosilicates, and aluminophosphates) have attracted considerable attention. Although the fact that trivalent iron occupies the tetrahedral site in zeolitic framework was established long ago, McNicol and Pott [10] showed in 1972 that the iron impurities in faujasite occupy the substitutional framework sites. A detailed synthesis, characterization, and description of the catalytic properties of a ferrisilicate with MFI structure were first published in 1985 [11]. The isomorphous substitution of trivalent iron in the framework structure of many silicate and aluminosilicate topologies, including ZSM-5, ZSM-11, ZSM-12, ZSM-23, EU-1, EU-2, zeolite-L, sodalite, beta, faujasite, and mordenite have also been reported [12,13]. The isomorphous substitution of trivalent iron in aluminophosphate molecular sieves with APO-5, APO-11, and VPI has also been published [14–17]. All of these catalysts have been used in

* Corresponding author. Fax: +91 22 2572 3480.
E-mail address: selvam@chem.iitb.ac.in (P. Selvam).

0021-9517/$ – see front matter
doi:10.1016/j.jcat.2005.12.005

numerous catalytic reactions, including the oxidation of cyclohexane and phenol and the Prins condensation reaction [18–22].

The small pore opening of these microporous materials restricts their use in processes with bulky molecules, however. Although the trivalent iron-substituted mesoporous silica molecular sieves [23–33] showed much promise for large molecules, they have the same disadvantages as the microporous materials. A major problem with both microporous and mesoporous molecular sieve-based materials is the instability of trivalent iron in the tetrahedral framework during heat treatment. This problem is well documented in the literature and, hence the application of iron-substituted molecular sieves has been limited, in contrast to many other transition metal-containing molecular sieves. To the best of our knowledge, no one has reported the synthesis of trivalent iron-substituted hexagonal mesoporous aluminophosphate (FeHMA) molecular sieves. These sieves are similar to the mesoporous silicates/aluminosilicates in that they have the MCM-41 structure [34–38]. Compared with the silicates/aluminosilicates, the low pH synthesis and the flexible network of HMA are the main factors favoring stabilization of large amounts of trivalent iron in the matrix. Here we give a detailed account of the synthesis, characterization, and catalytic properties of FeHMA. A preliminary description of this work was given elsewhere [39]. For comparison, we also studied mesoporous iron-substituted silicate (FeMCM-41) as well as microporous iron-substituted aluminophosphate (FeAPO-5) and silicate (FeS-1) catalysts.

The development of environmentally benign catalytic oxidation processes with eco-friendly oxidants such as hydrogen peroxide, molecular oxygen, and air under mild reaction conditions is of immense industrial importance [40,41]. In recent years, several groups have described a number of promising heterogeneous catalysts for the oxidation of cyclohexane [42–45]. No reports are available on the oxidation of higher cycloalkanes such as cyclooctane and cyclododecane, in contrast to homogeneous catalysts for the oxidation of these bulky cycloalkane molecules. But low yields, longer reaction periods, deactivation of the catalysts through the oxidative degradation of ligands, problems with separation, and the production of hazardous byproducts have made these catalysts uninteresting [46–48]. In this investigation, we used trivalent iron-substituted hexagonal mesoporous aluminophosphate (FeHMA) molecular sieves for the selective oxidation of cycloalkanes under mild reaction conditions. A preliminary account of the work has been published elsewhere [39].

2. Experimental

2.1. Starting materials

We used phosphoric acid (85%; Qualigens), aluminium isopropoxide (97%; Merck), tetramethyl ammonium hydroxide (TMAOH, 25 wt% in water; Aldrich), cetyltrimethylammonium chloride (CTAC, 25 wt% in water; Aldrich), CABOT fumed silica (99.8%; Aldrich), cetyltrimethylammonium bromide (CTAB, 99%; Aldrich), sodium hydroxide (NaOH, 98%; Loba), ferric nitrate (>98%; Aldrich), triethylamine (99.5%; Thomas Baker), pseudoboehmite (70%; Vista), tetrapropylammonium bromide (TPAB, 98%; Lancaster), cyclohexane (99.5%; Merck), *tert*-butyl hydroperoxide (TBHP, 70% aqueous solution; Lancaster), cyclooctane (99%; Lancaster), cyclododecane (99%; Lancaster), methyl ethyl ketone (MEK, 99.5%; SD fine), and glacial acetic acid (>99%; Fischer).

2.2. Hydrothermal synthesis

2.2.1. FeHMA

The synthesis was carried out as follows. Phosphoric acid (1.4 mL) was diluted with 11.7 mL of water. Then 4.08 g of aluminium isopropoxide was added under vigorous stirring, followed by the addition of an iron nitrate solution (0.378 g in 5 mL of water). The mixture was stirred for 1 h at 343 K, after which TMAOH (7.3 mL) was added dropwise. The slurry was stirred for few hours, then drops of CTAC (13.2 mL) were added and the mixture was stirred for another 12 h. The pH of the gel was maintained at 10. The final gel, with a molar composition of $(1-x)$ Al_2O_3:P_2O_5:x Fe_2O_3:CTAC:2.8 TMAOH:70 H_2O, was kept in a Teflon-lined autoclave and heated in an air oven at 373 K for 6 days until crystallization. The resultant solid was washed repeatedly with distilled water, filtered, and dried at 343 K for 12 h. Calcination was performed at 823 K for 1 h in a flow of N_2 and for 2 h in air. By varying the value of x, we prepared samples of varying molar ratios ([Al + P]/Fe): FeHMA(200), FeHMA(100), FeHMA(50), and FeHMA(25).

2.2.2. FeMCM-41

The synthesis was carried out as described previously [24]. First, TMAOH was dissolved in water, and the mixture was stirred for 15 min. Fumed silica was added slowly (solution A). Another mixture was prepared by mixing CTAB and NaOH in distilled water and stirring it for 30 min (solution B). Solution A was then added dropwise to solution b, and the resulting gel was stirred for 1 h to achieve homogenization. Acidified ferric nitrate solution was added dropwise to the gel to prevent the precipitation of iron; the pH of the gel was maintained at about 11.3–11.5. The final (molar) gel composition was 1 SiO_2:0.27 CTAB:0.26 NaOH:0.26 TMAOH:60 H_2O:0.01 Fe_2O_3 (Si/Fe = 50). The gel was transferred to Teflon-lined stainless steel autoclaves and kept in an air oven for crystallization at 423 K for 216 h. The solid products were washed, filtered, and dried in an oven at 353 K for 12 h. The as-synthesized samples were calcined at 823 K in a flow of N_2 for 2 h and in air for 8 h.

2.2.3. FeAPO-5

The synthesis was performed according to the following procedure. Pseudoboehmite (13.1 g) was hydrolyzed in 20 mL of distilled water for 2 h until a slurry was obtained. Phosphoric acid (13.2 mL) was added dropwise to this slurry, which was stirred for 2 h until a homogeneous gel was obtained. During stirring, 1.84 g of ferric nitrate, dissolved in 10 mL of acidified water, was added dropwise to the homogeneous gel for 1 h. The organic template, 36 mL of TEAOH, was added dropwise, and the mixture was stirred vigorously for 3 h. The final gel (0.09 Al_2O_3:0.1 P_2O_5:0.1 TEAOH:0.0038 Fe_2O_3:4 H_2O; [Al +

P]/Fe = 50), with a pH of 3.8, was subjected to a hydrothermal treatment at 423 K for 24 h in a Teflon-lined autoclave. The as-synthesized sample was calcined at 873 K in air for 10 h.

2.2.4. FeS-1

The synthesis with done with a typical molar gel composition of 1 SiO_2:0.5 Na_2O:1 TPAB:0.01 Fe_2O_3:100 H_2O (Si/Fe = 50) and a pH of 11.8. The gel was prepared by mixing fumed silica (4.0 g), acidified ferric chloride (4.84 g) solution, TPAB (17.3 g), sodium hydroxide (2.6 g), and water (120 mL) for several hours. Crystallization of the gel was carried out in a Teflon-lined autoclave at 453 K for 192 h under static conditions. The as-synthesized samples were calcined at 823 K for 12 h under air.

All of the as-synthesized FeHMA samples with different [Al + P]/Fe (molar) ratios as well as the as-synthesized FeMCM-41, FeAPO-5, and FeS-1 with a [Al + P]/Fe (molar) ratio of 50 were white. The as-synthesized FeHMA(25), calcined FeHMA(25), FeMCM-41, FeS-1, and FeHMA(25) were off-white; the bulk Fe_2O_3 was brown; and the metal-free HMA, MCM-41, APO-5, and S-1 were white.

2.3. Characterization

All of the as-synthesized and calcined samples were systematically characterized using various analytical and spectroscopic techniques. Powder X-ray diffraction (XRD) patterns were recorded on a Rigaku-Miniflex diffractometer using Ni-filtered Cu-K_α radiation ($\lambda = 1.5418$ Å) and a step size of 0.02°. Transmission electron microscopy (TEM) images were recorded on a Philips 200 microscope operated at 160 kV. The fine-powder sample was dispersed in ethanol with sonication (Oscar Ultrasonics); a drop of this solution was placed on a carbon-coated copper grid (300 mesh; Sigma-Aldrich). Elemental analysis of the samples was done by inductively coupled-plasma atomic emission spectroscopy (ICP-AES) using a Labtam Plasma Lab 8440 instrument. Thermogravimetry/differential thermal analysis (TG/DTA) measurements were performed with about 15 mg of the sample in a Dont 9900/2100 TG/DTA system in nitrogen atmosphere (40 mL min^{-1}) at a heating rate of 10 K min^{-1}. The catalyst was also subjected to temperature-programmed desorption (TPD) of ammonia. About 400 mg of sample was placed in quartz reactor and activated at 823 K in air for 6 h, followed by 2 h in helium with a flow rate of 50 mL min^{-1}. Then the reactor was cooled to 373 K and maintained for 1 h under the same conditions. Ammonia adsorption was carried out by passing the gas through the sample for 15–20 min at this temperature, followed by purging with helium for 1 h. The desorption of ammonia was carried out by heating the reactor to 873 K at a rate of 10 K min^{-1} using a temperature programmer (Eurotherm). The amount of ammonia desorbed was estimated with the aid of a thermal conductivity detector (TCD) response factor for ammonia. The ammonia desorption profile was deconvoluted using a Gaussian function with temperature as the variant.

Surface area analysis was performed with a Sorptomatic 1990 instrument. Before measurement, the calcined sample was evacuated at 523 K for 12 h under vacuum (10^{-3} Torr). Surface area (S_{BET}) was determined by the Brunauer–Emmett–Teller (BET) calculation, and pore size was determined by the Horvath–Kawazoe (HK) method. The pore volume was determined from the amount of nitrogen adsorbed at $p/p_0 = 0.5$. Diffuse-reflectance ultraviolet–visible (DRUV–vis) spectra were recorded on a UV-260 Shimadzu spectrophotometer with Whatman-40 filter paper as the standard. Fourier transform infrared spectra of the samples were recorded in the mid-infrared (IR) region (4000–400 cm^{-1}) using a Nicolet Impact 400 spectrometer at a resolution of 4 cm^{-1} and with 128 scans using the KBr pellet technique. About 100 mg of dry KBr was ground with 10 mg of the sample until the mixture was homogeneous and then dried using an IR lamp. The fine powder was then pressed into a transparent thin pellet at 5 tons cm^{-2}. These pellets were used for the IR spectral measurements. EPR spectra (X-band) of all of the materials were recorded both at room temperature (298 K) and at liquid nitrogen temperature (77 K) on a Varian (E-line Century series E-112) spectrometer with 100-kHz field modulation. The magnetic field was calibrated with a proton resonance meter and tetracyanoethylene ($g_{eff} = 2.0077$) as a reference. Mössbauer spectra were recorded in transmission geometry by placing the sample inside a variable-temperature bath cryostat. A ^{57}Co source in an Rh matrix and a proportional counter were used for these measurements. The velocity was chosen to accommodate the full velocity range of the spectrum. Assuming a Lorenzian line shape, the spectra were fitted via a least squares method using the computer program NORMOS.

2.4. Catalytic activity

The activity of the various catalysts was evaluated for the oxidation reactions of cycloalkanes. The oxidation reaction was carried out using 18 mmol of cyclohexane in 5 mmol of initiator (MEK) at 373 K for 12 h under ambient pressure using 50 mg of catalyst with 18 mmol of oxidant (30% H_2O_2) and 10 mL of solvent (acetic acid). The influence of the oxidants air, oxygen, and TBHP on the reaction was also investigated. The oxidation of cyclooctane (18 mmol) and cyclododecane (12 mmol) were carried out under similar conditions, except with mixed solvents (5 mL of acetic acid + 5 mL of dichloromethane) used to achieve a homogeneous reaction mixture. The catalyst was filtered after the reaction, washed three times with distilled water, dried in an air oven, activated at 773 K for 6 h, and used for subsequent recycling studies. After the reaction, the catalyst was separated, and the products were extracted with ether and analyzed in a gas chromatograph (Nucon) in a Carbowax column. Further identification of the oxidation products was confirmed by combined gas chromatography–mass spectrometry (GC–MS) using a Hewlett Packard G1800A equipped with an HP-5 capillary column.

Table 1
XRD and ICP-AES data of various iron-containing molecular sieves

Sample[a]	a_0 (Å)		Composition[b]			
	As-synthesized	Calcined	Al/P	[Al + P]/Fe	Si/Fe	Fe (wt%)
HMA	45.4	33.7		–	–	–
FeHMA(200)	45.6	36.0	1.31	170	–	0.65
FeHMA(100)	46.5	36.7	1.30	75	–	1.47
FeHMA(50)	47.3	36.8	1.29	40	–	2.30
FeHMA(25)	47.8	38.5	1.28	27	–	3.10
APO-5	13.68	13.61	1.00	–	–	–
FeAPO-5(50)	13.71	8.42	0.98	37	–	1.95
MCM-41	46.6	40.4	–	–	–	–
FeMCM-41(50)	57.9	51.2	–	–	42	2.10
S-1	20.07	19.98		–	–	–
FeS-1(50)	20.11	19.98	–	–	45	1.90

[a] Number in parentheses indicates the nominal [Al + P]/Fe or Si/Fe ratio.
[b] For calcined samples.

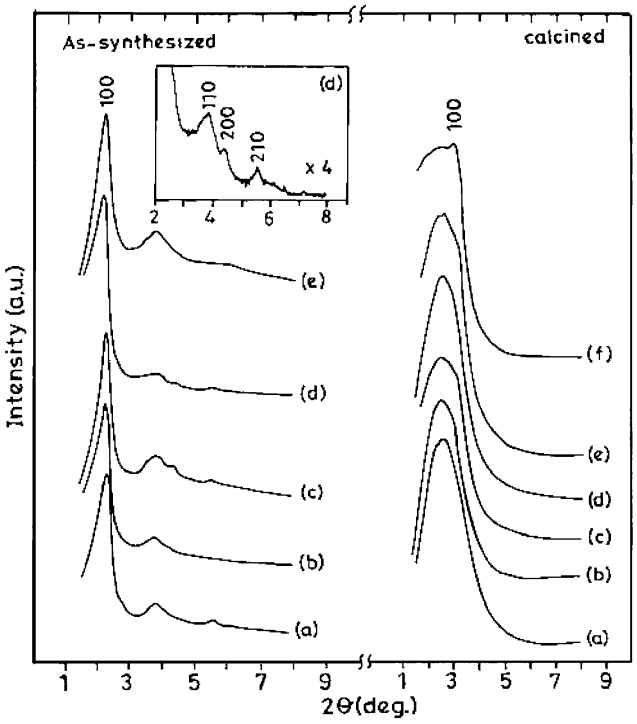

Fig. 1. XRD patterns of (a) HMA, (b) FeHMA(200), (c) FeHMA(100), (d) FeHMA(50), (e) FeHMA(25), and (f) FeHMA(50) after cyclohexane oxidation.

3. Results and discussion

3.1. Mesopore structure

XRD patterns of all of the as-synthesized FeHMA samples (Fig. 1) show features characteristic of the hexagonal crystal system [34–38]. On calcination, the unit cell dimension (Table 1) decreased for all of the samples as a consequence of the removal of the surfactant from the mesopores. Furthermore, the 110, 200, and 210 reflections disappeared, and only a broad single reflection, corresponding to the (100) plane, was observed. Similar observations were also reported for HMA, and it was concluded that this was probably due to the finite size

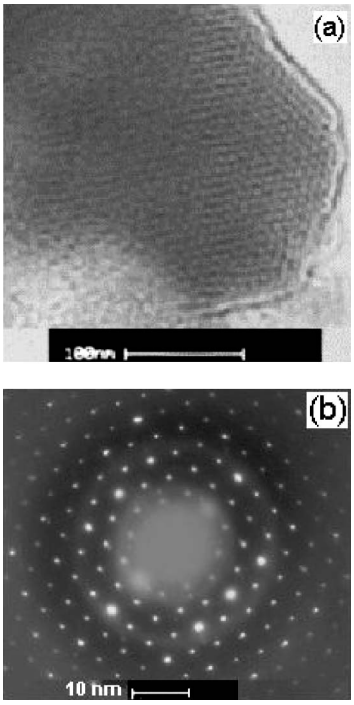

Fig. 2. (a) TEM and (b) ED of calcined FeHMA(50).

effects of very fine particle morphology or to the disordered structure [49–51]. The results are strongly supported by the TEM image and ED pattern of calcined HMA showing a disordered hexagonal pattern (Fig. 2). Thus it is concluded that mesoporous aluminophosphate materials belong to the disordered materials with a tubular pore system. At this juncture, it is noteworthy that the single broad reflection was also observed for hexagonal mesoporous silica (HMS), synthesized by neutral templating [49], and for disordered mesoporous MSU-1 silica materials, synthesized by neutral assembly using a nonionic poly(ethyleneoxide) surfactant, KIT-1 [50], prepared by electrostatic templating in the presence of tetrasodium salt of ethylenediaminetetraacetic acid [51]. But the materials produced in this study show greater disorder than the materials reported in the literature. Fig. 3 depicts the XRD patterns of different FeMCM-41 samples, which exhibit well-defined reflections typical of the hexagonal MCM-41 structure. The XRD patterns of FeAPO-5 and FeS-1 (not reproduced here) showed well-crystallized AFI and MFI topology, respectively [12,17].

TG of all of the as-synthesized FeHMA samples demonstrated a total weight loss of about 60–65% of three different stages, corresponding to adsorbed water molecules, template, and TMA ions [45]. The calcined FeHMA samples showed a weight loss of 20–23% due to the adsorbed water/gaseous molecules with a corresponding endotherm at 473 K in DTA, indicating the mesoporous nature of the samples. It also indicates complete removal of the templates by thermal calcinations. A representative TG/DTA trace, along with a NH_3-TPD profile of calcined FeHMA(50), are displayed in Fig. 4. The first peak at around 373–423 K (Fig. 4b) is attributed to weak acid sites originating from surface hydroxyl groups (defect sites), whereas the peaks at 423–623 K originate from moderate to

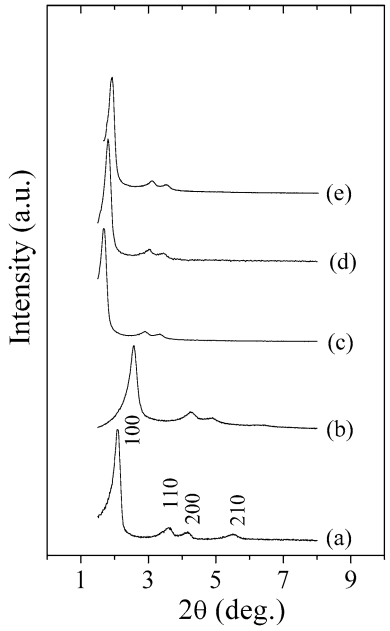

Fig. 3. XRD patterns of (a) as-synthesized MCM-41, (b) calcined MCM-41, (c) as-synthesized FeMCM-41(50), (d) calcined FeMCM-41(50), and (e) calcined FeMCM-41(50) after cyclohexane oxidation.

Table 2
Topology data of calcined FeHMA and FeMCM-41

Sample[a]	Surface area ($m^2\ g^{-1}$)	Pore volume ($ml\ g^{-1}$)	H-K pore diameter (Å)	FWT (Å)[b]
HMA	985	0.47	25	8.7
FeHMA(200)	975	0.48	26	10.0
FeHMA(100)	950	0.50	27	9.7
FeHMA(50)	923	0.48	28	8.8
FeHMA(50)[c]	940	0.50	28	9.2
FeHMA(25)	890	0.43	28	10.5
MCM-41	1080	0.80	30	10.4
FeMCM-41(50)	637	0.50	33	18.2

[a] Number in parentheses indicates the nominal [Al + P]/Fe or Si/Fe ratio.
[b] Framework wall thickness (FWT) = a_0 − H-K pore diameter.
[c] Spent catalyst.

strong structural acid sites, plausibly due to the presence of two different ions, Al^{3+} and P^{5+}, with distinct electronegativities. This view is consistent with the TG/DTA data showing that the adsorbed water molecule desorbs at 323–423 K. On the other hand, the peak at higher temperature (823–923 K) is assigned to the presence of tricoordinated aluminium/iron or octahedral aluminium/iron oxide or oxyhyroxide species present in the matrix due to incomplete condensation of Al–O–P/Fe–O–P network.

Nitrogen adsorption–desorption (sorption) analysis confirmed the mesoporous nature of all of the samples (Table 2). A representative nitrogen sorption isotherm of FeHMA(50) is shown in Fig. 5. It follows the type IV isotherm, typical of mesoporous materials [52,53]. As the relative pressure increases ($p/p_0 > 0.2$), the isotherms exhibit an inflection characteristic of capillary condensation within the mesopores. Adsorption at low relative pressures ($p/p_0 < 0.2$) is caused by monolayer adsorption of N_2 on the walls of the mesopores

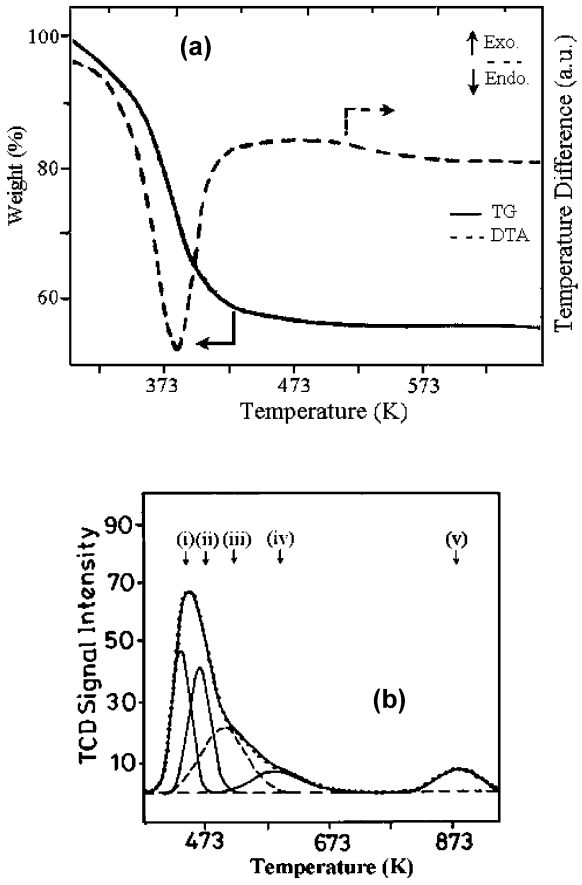

Fig. 4. (a) TG/DTA of calcined FeHMA(50). (b) NH_3-TPD of calcined FeHMA(50).

[52,53]. At $p/p_0 = 0.5$, the pore volume was 0.48 $cm^3\ g^{-1}$ with a specific surface area of 923 $m^2\ g^{-1}$. A narrow pore size distribution was observed (Fig. 5, inset) with a mesopore diameter of 28 Å. These values are close to the surface parameters of HMA (surface area, 985 $m^2\ g^{-1}$; pore volume, 0.47 $cm^3\ g^{-1}$; pore diameter, 25 Å), indicating the absence of nonframework iron oxides inside the pore. In contrast, a significant decrease in surface area was observed in FeMCM-41 (637 $m^2\ g^{-1}$) compared with Fe-free MCM-41 (1080 $m^2\ g^{-1}$). The FTIR spectra of the as-synthesized samples (not reproduced here) showed the characteristic bands corresponding to the mesoporous aluminophosphate matrix and the template molecules. The calcined samples exhibit almost complete removal of the template molecules (absence of peaks at 2827, 2861, and 1480 cm^{-1}) from the as-synthesized sample. All of the above results clearly demonstrate the hexagonal structure and mesoporosity of FeHMA.

3.2. Nature of iron species

In molecular sieve-based catalysts, the nature/coordination of the iron species is very important from the standpoint of catalysis, in which the adsorption of the substrates generally occurs on these sites. In particular, iron is known to exist in many forms, including isolated Fe^{2+}/Fe^{3+} species, various iron oxides, hydroxides, and oxyhydroxides. Hence, distinguishing the various species by a specific technique is very difficult. To

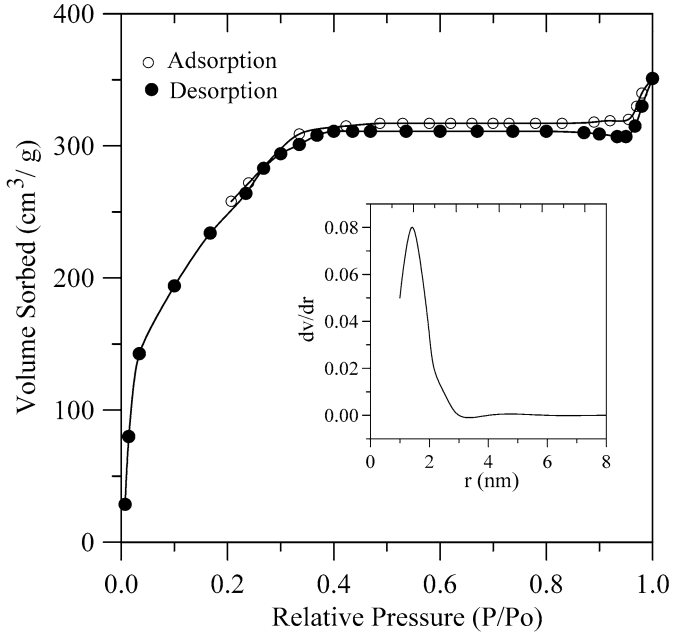

Fig. 5. N_2 sorption isotherm of calcined FeHMA(50) (inset: pore size distribution).

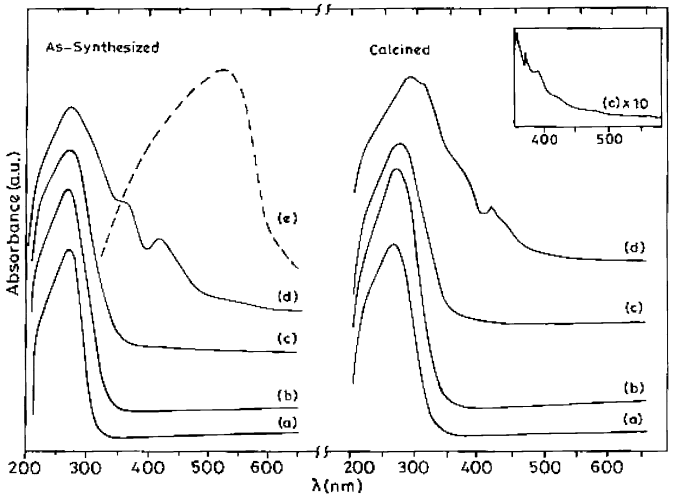

Fig. 6. DRUV–vis spectra of (a) FeHMA(200), (b) FeHMA(100), (c) FeHMA (50), (d) FeHMA(25), and (e) bulk Fe_2O_3.

distinguish these very different species, we used several characterization techniques. These methods were particularly useful in demonstrating the isomorphous substitution of iron species in the matrix. Furthermore, a major problem associated with both microporous and mesoporous silicate materials is the instability of trivalent iron in the tetrahedral framework during heat treatment. Thus, in contrast to many other transition metal-containing silicate molecular sieves, the application of iron-substituted molecular sieves has been limited, and hence it is necessary to use various characterization techniques to demonstrate the stability of trivalent iron in the matrix.

Fig. 6 shows the DRUV–vis spectra of various iron-containing as-synthesized and calcined FeHMA samples. The FeHMA (200), FeHMA(100), and FeHMA(50) samples showed two prominent bands (a strong band at ∼290 nm associated with a shoulder at 230 nm) in the UV region, explaining the Laporte-allowed ligand-to-metal charge-transfer transitions ($t_1 \rightarrow t_2$ and $t_1 \rightarrow e$) involving Fe^{3+} in $[FeO_4]^-$ tetrahedral geometry [54–56]. None of the samples exhibited significant absorption above 350 nm, indicating that the as-synthesized FeHMA samples were free of octahedral iron species (iron hydroxide, iron oxyhydroxide, and iron oxide clusters). In contrast, the spectrum of as-synthesized FeHMA(25) contained broad transitions in the 350–500 nm range. This increase in the spectra broadening with increasing iron concentration of the FeHMA samples indicates that after a certain time, iron may shift to the extra-framework lattice position. Fig. 6 also shows that the spectra of the corresponding calcined FeHMA samples were similar to their as-synthesized analogues. The weak bands in the 350–500 nm region (Fig. 6, inset) are assigned to spin-forbidden d–d transitions, originate from a weak crystal field in the calcined sample, and indicate the stability of the tetrahedral iron in the FeHMA matrix [54–56]. These bands are usually considered to strongly indicate a tetrahedral environment of Fe^{3+} species in zeolite frameworks [57]. The spectrum of the as-synthesized FeMCM-41 sample (Fig. 7b) showed similar transitions to that of as-synthesized FeHMA (Fig. 7a) corresponding to Fe^{3+} in a tetrahedral network. However, after calcination, the FeMCM-41 (Fig. 8b) spectra broadened considerably in the case of the former (with the sample color also changing from white to off-white), leading to the disappearance of the weak d–d transitions corresponding to Fe^{3+} ions in the tetrahedral network. This clearly indicates a change in the coordination/environment around Fe^{3+} in FeMCM-41 materials. This broadening of the spectrum corresponds to a possible shift of some of the framework Fe^{3+} ions to the extra-framework lattice during calcination [54]. Similar findings were also observed for FeS-1.

Fig. 9 depicts the ESR spectra of as-synthesized FeHMA samples at room temperature (298 K) and liquid nitrogen temperature (77 K). The as-synthesized FeHMA(200), FeHMA (100), and FeHMA(50) samples showed a strong signal at $g_{\text{eff}} = 4.3$, assigned to high-spin Fe^{3+} in the distorted tetrahedral environment, and a very weak (or no) signal at $g_{\text{eff}} = 2.0$, attributed to high-spin Fe^{3+} in a symmetrical tetrahedral/octahedral coordination [54–56]. The intensity of the signal at $g_{\text{eff}} = 4.3$ increased sharply (4- to 5-fold) at 77 K, suggesting that the ions were in an isolated tetrahedral environment. Similar findings were observed for calcined samples (Fig. 10). In contrast, as-synthesized FeHMA(25) showed a distinct signal at $g_{\text{eff}} = 2.0$, but this signal was weak compared with the signal at $g_{\text{eff}} = 4.3$. The spectra of the calcined FeHMA samples did not change significantly, but the intensity of the signal at $g_{\text{eff}} = 2.0$ increased for the other molecular sieves under investigation. This suggests that the Fe^{3+} ions in the FeHMA samples did not become dislodged from the matrix even after calcination; these results are in line with results of DRUV–vis studies. The reused catalyst (for the oxidation of cyclohexane) also showed a similar ESR pattern and signal intensity as the parent calcined FeHMA(50) catalyst (Fig. 10e), confirming the stability of the iron species in the matrix under reaction conditions. FeMCM-41 showed two strong signals at

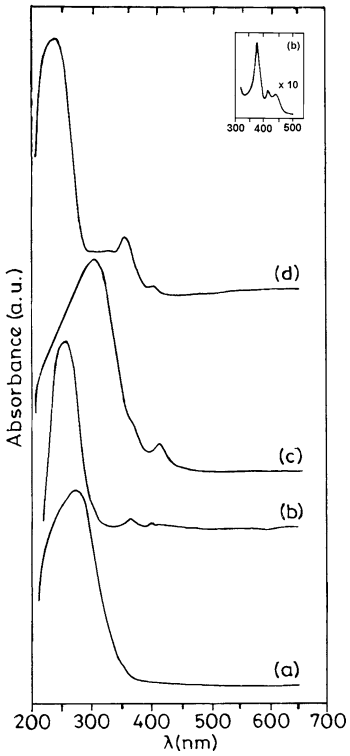

Fig. 7. DRUV–vis spectra of as-synthesized (a) FeHMA(50), (b) FeMCM-41(50), (c) FeAPO-5(50), and (d) FeS-1(50).

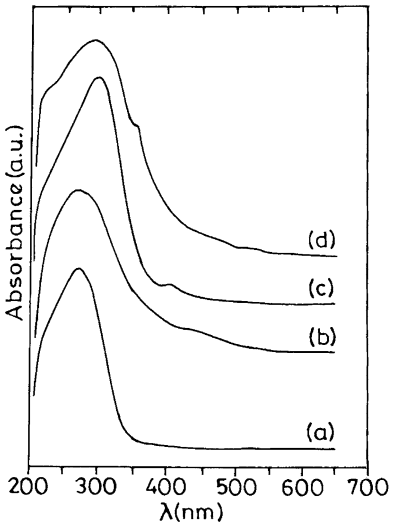

Fig. 8. DRUV–vis spectra of calcined (a) FeHMA(50), (b) FeMCM-41(50), (c) FeAPO-5(50), and (d) FeS-1(50).

$g_{\text{eff}} = 2.0$ and $g_{\text{eff}} = 4.3$ and a weak signal at $g_{\text{eff}} = 2.1$–2.3 (Fig. 11). The additional feature at $g_{\text{eff}} = 2.2$ was due mainly to the presence of nonframework (superparamagnetic) iron oxyhydroxide/oxide nanoparticles located inside the pores [58,59]. The change in color after calcination and the decrease in signal intensity at $g_{\text{eff}} = 4.3$ followed by the increased signal intensity at $g_{\text{eff}} = 2.0$ suggest that the signal at $g_{\text{eff}} = 4.3$ is due to tetrahedral substitution of Fe^{3+} ions in the molecular sieves and the signal at $g_{\text{eff}} = 2.0$ is due to the extra-framework iron in the matrix. Thus, these samples may contain octahedral iron species (even if not in bulk form). The intensity of the signal at $g_{\text{eff}} = 4.3$ decreases further after the reactions, reflecting the difference in stability of the iron species in the FeMCM-41 and FeHMA materials (although much speculation about these two signals persists). Thus, for comparison, we also give the spectrum of bulk Fe_2O_3 (Fig. 8e), which showed a broad signal at $g_{\text{eff}} = 2.0$. This supports our proposal that the signal at $g_{\text{eff}} = 2.0$ may contribute in part to the octahedral iron species. However, the signal at $g_{\text{eff}} = 4.3$ is unambiguously supported as the tetrahedral iron, because it increases sharply at low temperature (Curie–Weiss behavior), which is possible only for isolated paramagnetic species [16]. Similar findings were also observed for FeS-1 (spectra not reproduced here).

Table 3
Mössbauer data of various FeHMA

Sample[a]	T (K)	Subspectra[b]	δ[c] (mm s^{-1})	ΔE[d] (mm s^{-1})	Relative area (%)
FeHMA(100)[e]	298	I	0.04	0.48	95
		II	0.52	1.56	5
FeHMA(50)[f]	298	I	0.15	0.76	89
		II	0.56	2.50	11
FeHMA(50)[e]	298	I	0.17	0.69	93
		II	0.62	2.10	7
	77	I	0.25	0.72	93
		II	0.85	1.90	7
	4.2	I	0.31	0.66	97
		II	0.81	2.35	3
FeHMA(25)[e]	298	I	0.34	0.76	90
		II	0.79	2.80	10

[a] Number in parentheses indicates the nominal [Al + P]/Fe or Si/Fe ratio.
[b] I, strong doublet; and II, weak doublet.
[c] Isomer shift.
[d] Quadruple splitting.
[e] Calcined.
[f] As-synthesized.

To gain further insight into the state of iron, we carried out ^{57}Fe Mössbauer studies at different temperatures. Discrimination between framework and extra-framework iron species in zeolites by Mössbauer spectroscopy is usually made on the basis of the isomer shift (IS). At room temperature, an IS < 0.3 mm s^{-1} with narrow quadruple splitting (QS) indicates tetrahedral Fe^{3+} ions, whereas IS > 0.3 mm s^{-1} with broad quadruple splitting characterizes six-coordinated iron species [12]. Figs. 12 and 13 show the Mössbauer spectra of various FeHMA samples; more detailed information is given in Table 3. The room temperature Mössbauer spectrum of all of the samples can be fitted by two doublets, a narrow one (subspectrum I) assigned to high-spin Fe^{3+} and a wide one (subspectrum II) assigned to high-spin Fe^{2+}, with the latter having higher IS and QS values than the former. In all of the samples, subspectrum I is very intense compared with subspectrum II, indicating that in all of these samples, Fe^{3+} species predominate and the amount of Fe^{2+} is around 10%. Table 3 lists various parameters of the Mössbauer studies for all of the iron-containing samples. The IS values of the subspectra I of FeHMA(200), FeHMA(100) and FeHMA(50) are <0.3 mm s^{-1}, confirming the tetrahedral substitution of iron in these samples. It is noteworthy that the values of the calcined samples are similar to

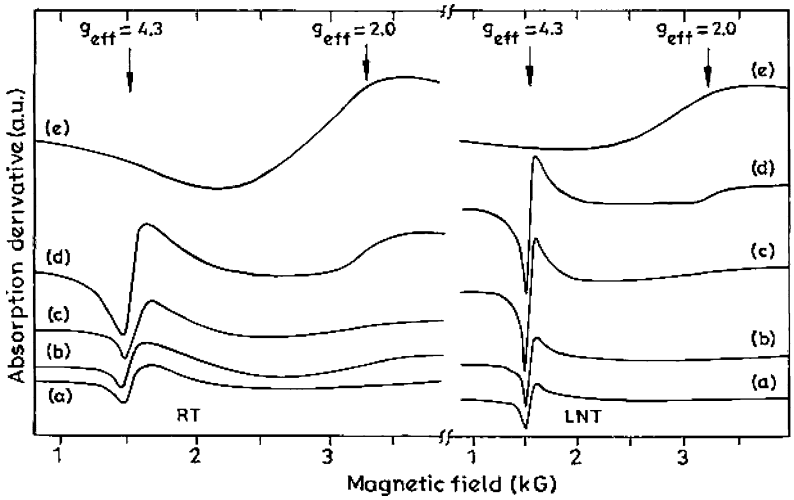

Fig. 9. ESR spectra of as-synthesized (a) FeHMA(200), (b) FeHMA(100), (c) FeHMA(50), (d) FeHMA(25), and (e) bulk Fe_2O_3.

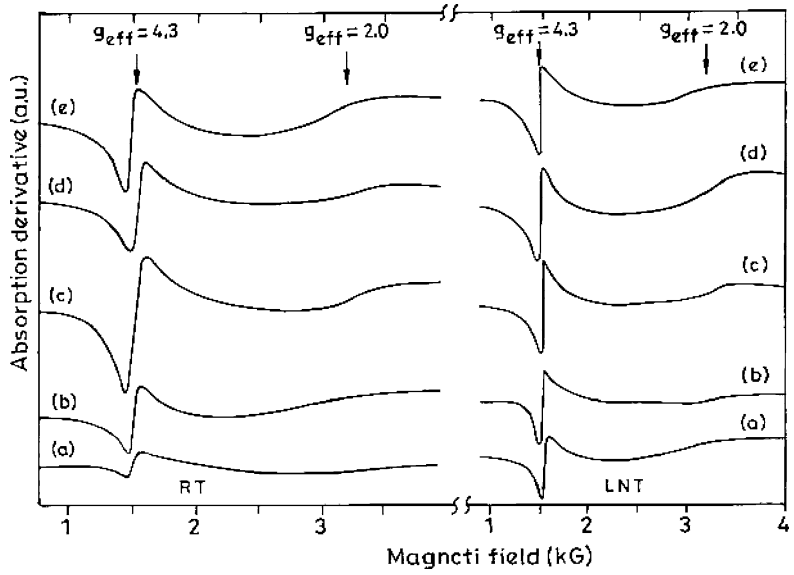

Fig. 10. ESR spectra of calcined (a) FeHMA(200), (b) FeHMA(100), (c) FeHMA(50), (d) FeHMA(25), and (e) calcined FeHMA(50) after cyclohexane oxidation.

those of the as-synthesized samples, an indication of the exceptional stability of iron in the tetrahedral matrix. The presence of the minor QS indicates that the Fe^{3+} ions in the FeHMA lattice deviate from the ideal tetrahedral symmetry [15–17]. The weak doublet (subspectra II) is attributed to Fe^{2+} ions in tetrahedral coordination, originating from the reduction of Fe^{3+} during synthesis [15–17].

The calcined FeHMA(50) catalyst was taken as a representative sample to study the effect of various temperatures (Fig. 13). The spectrum of FeHMA(50) at 77 K can be fitted with two doublets, similar to the spectrum at 298 K. A similar spectrum is also observed at 4.2 K. The increase in IS values with decreasing temperature is due to the second-order Doppler effect (Table 4). The absence of the sextet pattern at low temperature (4.2 K) confirms the absence of iron oxide superparamagnetic particles inside the pores of the FeHMA material. For comparison, the spectra of FeMCM-41 are also shown in Fig. 14. A similar tetrahedral coordination of Fe^{3+} ion was also observed for as-synthesized FeMCM-41, but after calcination, the increase in IS (>0.3) indicates the formation of octahedral ferric ions (Table 4). This is further confirmed by the sextet pattern obtained at 4.2 K in the spectra of calcined FeMCM-41, which

Table 4
Mössbauer data of FeMCM-41(50)[a]

Sample[a]	T (K)	Subspectra[b]	δ[c] (mm s^{-1})	ΔE[d] (mm s^{-1})	Relative area (%)
As-synthesized	298	I	0.19	0.68	88
		II	0.81	3.20	12
Calcined	298	I	0.32	0.90	94
		II	0.95	2.80	6
	4.2	I	0.43	1.03	67
		III	0.50	0.0	33

[a] Number in parentheses indicates the nominal [Al + P]/Fe or Si/Fe ratio.
[b] I, strong doublet; II, weak doublet; III, sextet.
[c] Isomer shift.
[d] Quadruple splitting.

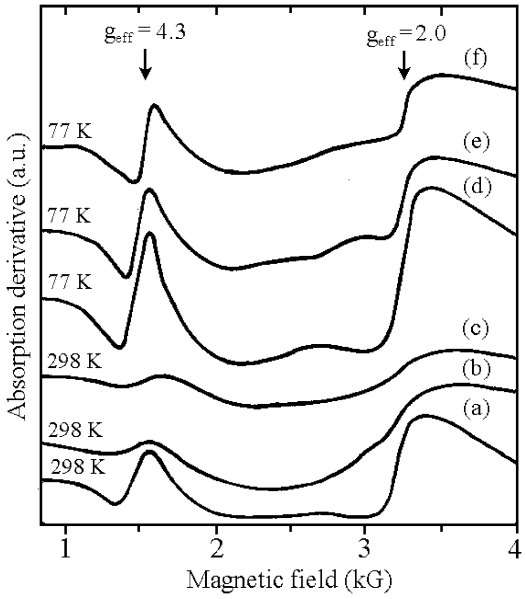

Fig. 11. ESR spectra of: (a), (d) as-synthesized FeMCM-41(50); (b), (e) calcined FeMCM-41(50); (c), (f) calcined FeMCM-41(50) after cyclohexane oxidation.

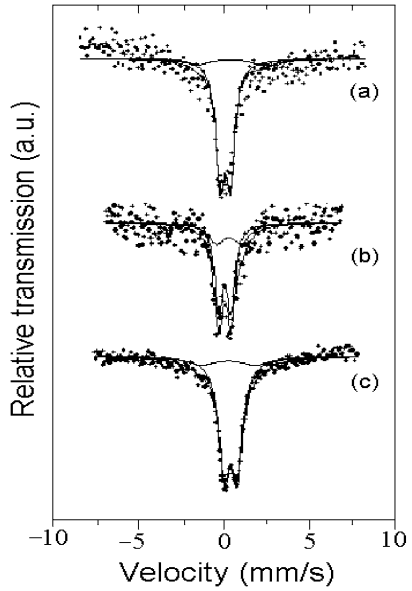

Fig. 12. Mössbauer spectra of (a) as-synthesized FeHMA(50), (b) calcined FeHMA(100), and (c) calcined FeHMA(25) at 298 K.

was absent in the calcined FeHMA material. Thus, these complementary techniques clearly reveal that in the mesoporous aluminophospate matrix, iron exists as Fe^{3+} (to a larger extent) and Fe^{2+} (to a lesser extent), both of which are tetrahedrally coordinated with O^{2-}. This conclusion is further substantiated by the ICP-AES results for FeHMA (see Table 1), in which a decrease in Al/P ratio with increasing iron content indicates isomorphous substitution of Fe^{3+} in the matrix. A similar trend was also noted earlier for the substitution of Fe^{3+} for Al^{3+} APO-5 topology [14]. In contrast, the decreased molar ratios in the calcined samples compared with the starting gel composition indicates that part of aluminum and/or phosphorous is lost in the mother liquor during synthesis.

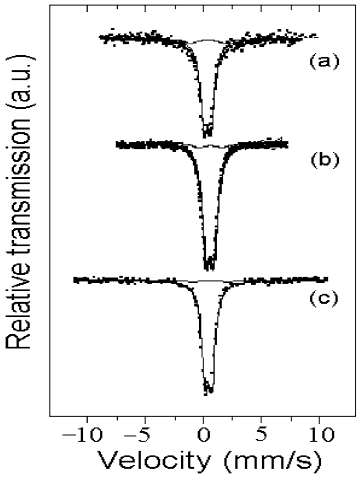

Fig. 13. Mössbauer spectra of calcined FeHMA(50) at (a) 298 K, (b) 77 K, and (c) 4.2 K.

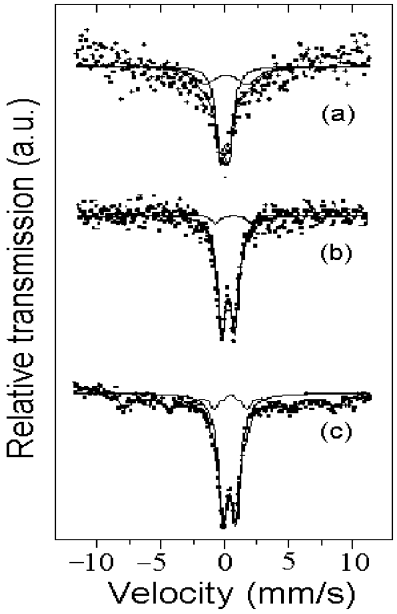

Fig. 14. Mössbauer spectra of (a) as-synthesized FeMCM-41(50) at 298 K, (b) calcined FeMCM-41(50) at 298 K, and (c) calcined FeMCM-41(50) at 4.2 K.

3.3. Catalytic activity

The results of the catalytic oxidation of cyclohexane over various iron-containing HMA catalysts show that cyclohexane conversion increased with increasing amounts of iron in the catalyst (Table 5). All of the catalysts produced two primary products, cyclohexanol and cyclohexanone. Of the secondary products, cyclohexyl acetate was predominant. With HMA, the reaction exhibited only about 10% cyclohexane conversion, similar to the reaction without catalyst (blank). Fe_2O_3 demonstrated 26% cyclohexane conversion under similar reaction conditions (Table 5). Thus the observed high activity of FeHMA is attributed to the presence of isolated tetrahedral Fe^{3+} ions in the

Table 5
Effect of iron content in FeHMA on the oxidation of cyclohexane[a]

Catalyst[b]	Conversion (wt%)	Selectivity (wt%)			TON[d]
		Cyclohexanol	Cyclohexanone	Others[c]	
FeHMA(200)	48.0	92.0	7.0	1.0	1489
FeHMA(100)	72.0	89.9	8.8	1.3	996
FeHMA(50)					
Calcined	84.0	66.0	27.0	7.0	756
Recycled[e]	82.7	73.4	20.0	6.6	745
FeHMA(25)	89.0	62.0	28.0	10.0	579
HMA	9.8	82.8	1.3	15.9	–
Blank	9.0	78.1	0.0	21.9	–
Fe_2O_3	26.0	84.0	10.0	6.0	22

[a] Reaction conditions: substrate/oxidant (H_2O_2) = 1; catalyst, 50 mg (3.3 wt%); T = 373 K; time = 12 h. Catalyst (wt%) = [catalyst weight × 100]/[substrate weight + catalyst weight].
[b] Number in parentheses indicates the nominal [Al + P]/Fe or Si/Fe ratio.
[c] Mainly cyclohexyl acetate is obtained as chain-terminating product.
[d] Turn-over number, number of moles of cyclohexane converted per mole of iron.
[e] 3rd recycle or 4th run.

Table 6
Effect of oxidants on the oxidation of cyclohexane over FeHMA(50)[a,b]

Catalyst[b]	Conversion (wt%)	Selectivity (wt%)			TON[d]
		Cyclohexanol	Cyclohexanone	Others[c]	
H_2O_2	84.0	66.0	27.0	7.0	756
TBHP	75.4	30.0	64.5	5.5	633
O_2	62.7	62.2	34.0	3.8	564
Air	46.0	67.8	31.2	1.0	414

[a] Reaction conditions: substrate:oxidant (H_2O_2 or TBHP) = 1:1; air and O_2 flow rate 40 ml min^{-1}; catalyst 50 mg (3.3 wt%); solvent acetic acid (10 mL); MEK 5 mmol; temperature, 373 K; time, 12 h. Catalyst (wt%) = [catalyst weight × 100]/[substrate weight + catalyst weight].
[b] Number in parentheses indicates the nominal [Al + P]/Fe or Si/Fe ratio.
[c] Mainly cyclohexyl acetate is obtained as chain-terminating product.
[d] Turn-over number, number of moles of cyclohexane converted per mole of iron.

matrix and to the mild reaction conditions, that is, acetic acid as the solvent, MEK as the initiator, and H_2O_2 as the oxidant at 373 K for 12 h. Table 5 indicates that all of the FeHMA catalysts had good turnover numbers (TONs); the table also shows, however, that TON decreased with increasing iron content, indicating that the activity was not increasing at the same degree as the iron content in the catalyst. In other words, in the higher iron-containing FeHMA catalysts, all of the iron species are not accessible to the substrate (cyclohexane), due to the steric constraint environment around the active iron species. In addition, the iron incorporated in the interior of the framework (wall) structure may not be available for the substrate molecules. In contrast, bulk Fe_2O_3 had a very low TON, indicating that isolated tetrahedral iron species are vital for functionalization of C–H.

The reaction was also carried out with different oxidants: 70% TBHP, molecular oxygen, and air (Table 6). The reaction with H_2O_2 exhibited high conversion at high cyclohexanol selectivity. On the other hand, TBHP yielded cyclohexanone as the major product, because this oxidant is more reactive than H_2O_2 [60]. However, the conversion was lower than that of

Table 7
Oxidation of cyclooctane over various iron-containing catalysts[a]

Catalyst[b]	Conversion (wt%)	Selectivity (wt%)			TON[d]
		Cyclohexanol	Cyclohexanone	Others[c]	
FeHMA(50)					
Calcined	92.5	51.5	40.0	8.5	832
Recycled[e]	93.0	47.8	45.6	7.7	837
FeMCM-41(50)	82.6	47.0	41.2	11.8	790
FeAPO-5(50)	33.5	42.7	40.0	17.3	346
FeS-1(50)	29.0	44.0	36.8	19.2	306

[a] Reaction conditions: substrate:oxidant (H_2O_2) = 1:1; catalyst = 50 mg (2.48 wt%); solvent, acetic acid (5 ml) + CH_2Cl_2 (5 ml); MEK, 5 mmol; temperature, 373 K; time, 12 h. Catalyst (wt%) = [catalyst weight × 100]/[substrate weight + catalyst weight].
[b] Number in parentheses indicates the nominal [Al + P]/Fe or Si/Fe ratio.
[c] Mainly cyclooctyl acetate is obtained as chain-terminating product.
[d] Turn-over number, number of moles of cyclooctane converted per mole of iron.
[e] 3rd recycled or 4th run.

H_2O_2, possibly due to deactivation of the catalyst by the formation of *tert*-butanol from the decomposition of TBHP. When the reaction was carried out in O_2 and air, substrate conversion was low, with cyclohexanol as the main product. This may be due to the direct attack on cyclohexane by O_2, an endothermic process that impairs the activation of a process. To overcome this problem, various oxidants, including iodobenzene [61], hydrogen peroxide [62,63], and alkylhydroperoxide [64,65], have been in place of energy-consuming dioxygen activation. Of these oxidants, H_2O_2 is preferable because it is simple to handle, its coproduct (water) is environmentally friendly, the oxygen atom is very efficient, and it is versatile [66,67]. The FeHMA(50) catalyst was also tested for its reusability (Table 5). Interestingly, no significant loss in activity was noticed (up to three cycles), and the yield was practically unaffected during recycling experiments. The TON of the reused catalyst also remained nearly the same, suggesting that the ferric ions were intact in the framework with the same environment as that of the initial catalyst. These results clearly indicate that Fe^{3+} was stabilized in the mesoporous matrix and hence that FeHMA behaved truly as a heterogeneous catalyst. The stabilization of trivalent iron in the tetrahedral matrix was further confirmed by the ICP-AES analysis of the filtrate that detected no iron. Thus the ICP-AES results not only corroborate stability of trivalent iron, but also substantiate the absence of leaching of the active species from the mesoporous matrix. Most importantly, the catalyst retained its structure (Fig. 1f) and porosity (Table 2) even after the third recycling.

To exploit the mesoporosity of the FeHMA catalyst, the oxidation of bulkier cycloalkanes, cyclooctane (Table 7) and cyclododecane (Table 8), was also carried out. FeHMA(50) showed excellent activity and selectivity for these bulkier substrates. Comparing the results of cyclohexane oxidation to these substrates, decreased selectivity of the alcohols (cyclooctanol and cyclododecanol) was observed, due to the lower diffusion rate of the bulky cyclooctanol/cyclododecanol compared with cyclohexanol inside the mesopores. Thus overoxidation of

Table 8
Oxidation of cyclododecane over various iron-containing catalysts[a]

Catalyst[b]	Conversion (wt%)	Selectivity (wt%)			TON[d]
		Cyclohexanol	Cyclohexanone	Others[c]	
FeHMA(50)	94.8	48.2	42.1	9.7	568
FeHMA(50)[d]	93.5	47.0	45.3	8.7	561
FeMCM-41(50)	82.1	48.2	40.0	11.8	524
FeMCM-41(50)[e]	70.5	50.1	38.0	11.9	512
FeAPO-5(50)	31.3	45.7	41.2	13.1	215
FeS-1(50)	26.6	48.3	38.7	13.0	188

[a] Reaction conditions: substrate:oxidant (H_2O_2) = 1:1; catalyst, 50 mg (2.48 wt%); solvent (acetic acid 5 ml + CH_2Cl_2 5 ml); MEK, 5 mmol; temperature, 373 K; time, 12 h. Catalyst (wt%) = [catalyst weight × 100]/[substrate weight + catalyst weight].
[b] Number in parentheses indicates the nominal [Al + P]/Fe or Si/Fe ratio.
[c] Mainly cyclododecyl acetate is obtained as chain-terminating product.
[d] Turn over number, number of moles of cyclooctane converted per mole of iron.
[e] 3rd recycled or 4th run.

the cycloalkanols to cycloalkanones occurred. FeHMA showed true heterogeneity for these substrates as well.

For comparison, the oxidation of cyclododecane was also carried out over FeMCM-41, FeAPO-5, and FeS-1. FeAPO-5 and FeS-1 showed only very low activity due to the pore size restriction of these bulky substrates. This may be because the lower pore wall of FeHMA(50) is not as thick as that of FeMCM-41, thus enabling the active species of the former to interact more with the substrate molecules [68,69]. The activity decreased in the recycling studies, with a considerable amount of iron being leached (12%) into the reaction mixture. Thus FeHMA is a novel catalyst, with good activity and selectivity for the oxidation of cycloalkanes. We suppose that the reaction goes through the free radical mechanism in the same way as the reactions reported for other iron-containing catalysts [20,70]. Because both isolated Fe^{2+} and Fe^{3+} species are known to be active for C–H activation [71,72], determining the exact contribution of each of these species to the overall catalyst activity is very difficult. But because Fe^{3+} is the major species and has a higher oxidation ability than Fe^{2+}, we believe that the activity is due mostly to Fe^{3+} species. At this point, it is worth noting that CoHMA [73] also showed comparable activity for cycloalkane oxidation, but the -one/-ol ratio was much higher in FeHMA, and hence CoHMA is quite attractive.

4. Conclusion

In conclusion, iron-substituted mesoporous aluminophosphate molecular sieves were successfully synthesized. Various characterization techniques suggested the presence of isolated Fe^{3+} ions of distorted tetrahedral framework sites. These tetrahedral Fe^{3+} ions did not become dislodged during heat treatment, indicating the stability of Fe^{3+} ions in a tetrahedral matrix compared with many other molecular sieves. Mössbauer studies demonstrated that around 10% of the iron was present in these materials as Fe^{2+}, with most of the iron present as Fe^{3+}. The catalyst showed excellent activity and recyclability for the oxidation of cyclohexane under relatively milder reaction conditions. It was also demonstrated that FeHMA can be used for the oxidation of bulky cycloalkanes, such as cyclooctane and cyclododecane. These catalysts are viable alternatives to the homogeneous catalysts because of their easy recoverability and recyclability, hence opening up new possibilities for the iron-based heterogeneous oxidation reactions.

Acknowledgments

The authors thank SAIF/RSIC, IIT-Bombay, for the ICP-AES, TEM, ED, and ESR measurements. They also thank W. Keune and Mr. B. Sahoo for the Mössbauer studies and Dr. S. Chaudhury for the surface area measurements.

References

[1] J.B. Vincent, G.L. Oliver-Lilley, B.A. Averill, Chem. Rev. 90 (1990) 144.
[2] M.J. Rataj, J.E. Kauth, M.I. Donnelly, J. Biol. Chem. 261 (1991) 18684.
[3] B. Meunier, Chem. Rev. 92 (1992) 1411.
[4] T.G. Traylor, C. Kim, J.L. Richards, E. Xu, C.L. Perrin, J. Am. Chem. Soc. 117 (1995) 3468.
[5] M. Benz, A.M. van der Kraan, R. Prins, Appl. Catal. A 172 (1998) 149.
[6] M. Ai, K. Ohdan, J. Mol. Catal. A 159 (2000) 19.
[7] G.L. Elizarova, L.G. Matvienko, V.N. Parmon, Kinet. Catal. 41 (2000) 839.
[8] N. Perkas, Y. Wang, Koltypin, A. Gedanken, S. Chandrasekaran, Chem. Commun. (2001) 988.
[9] M. Stockmann, E. Konietzni, J.U. Notheis, J. Voss, W. Keune, W.E. Maier, Appl. Catal. A 208 (2001) 343.
[10] B.D. Mcnicol, G.T. Pott, J. Catal. 25 (1972) 223.
[11] P. Ratnasamy, R.B. Borade, S. Sivasanker, V.P. Shiralkar, S.G. Hegde, Acta Phys. Chem. 31 (1985) 137.
[12] P. Ratnasamy, R. Kumar, Catal. Today 9 (1991) 239.
[13] R.B. Borade, A. Clearfield, Chem. Commun. (1996) 2267.
[14] P. Wenquin, Q. Shilun, K. Quibin, W. Zhiyun, P. Shaoyi, F. Guochuan, T. Di, Stud. Surf. Sci. Catal. A 49 (1989) 281.
[15] A.F. Ojo, J. Dwyer, R.V. Parish, Stud. Surf. Sci. Catal. A 49 (1989) 227.
[16] S. Schubert, H.M. Ziethen, A.X. Trautwein, F. Schmidt, H. Li, J.A. Martens, P.A. Jacobs, Stud. Surf. Sci. Catal. 46 (1989) 735.
[17] J. Das, C.V.V. Satyanaryana, D.K. Chakrabarty, S.N. Piramanayagam, S.N. Shringi, J. Chem. Soc., Faraday Trans. 88 (1992) 3255.
[18] P.E. Dai, R.H. Petty, C.W. Ingram, R. Szostak, Appl. Catal. A 143 (1996) 101.
[19] E. Dumitriu, V. Hulea, I. Fechete, C. Catrinescu, A. Auroux, J. Lacaze, C. Guimon, Appl. Catal. A 181 (1999) 15.
[20] R. Raja, G. Sankar, J.M. Thomas, J. Am. Chem. Soc. 121 (1999) 11926.
[21] R. Byggningsbacka, N. Kumar, L.-E. Lindfors, Catal. Lett. 58 (1999) 231.
[22] Y.S. Bhat, S. Ali, J. Das, B.D. Bhatt, A.B. Halgeri, J. Mol. Catal. A 111 (1996) 307.
[23] Z.Y. Yuan, S.Q. Liu, T.H. Chen, J.Z. Wang, H.X. Li, J. Chem. Soc., Chem. Commun. (1995) 973.
[24] S.K. Badamali, P. Selvam, Stud. Surf. Sci. Catal. 113 (1998) 749.
[25] N. He, S. Bao, Q. Xu, Appl. Catal. A 169 (1998) 29.
[26] S.K. Badamali, A. Sakthivel, P. Selvam, Catal. Lett. 65 (2000) 153.
[27] M. Stockenhuber, M.J. Hudson, R.W. Joyner, J. Phys. Chem. B 104 (2000) 3370.
[28] Y. Wang, Q. Zhang, T. Shishido, K. Takehira, J. Catal. 209 (2002) 186.
[29] D. Nicholson, L. Bonneviot, Chem. Mater. 9 (1997) 1716.
[30] H. Kosslick, G. Lischke, H. Landmesser, B. Parlitz, W. Storek, R. Fricke, J. Catal. 176 (1998) 102.
[31] W. Zhao, Y. Luo, P. Deng, Q. Li, Catal. Lett. 73 (2001) 199.
[32] A. Tuel, L. Arcon, J.M.M. Millet, J. Chem. Soc., Faraday Trans. 94 (1998) 3501.
[33] Y. Han, X. Meng, H. Guan, Y. Yu, L. Zhao, X. Xu, X. Yang, S. Wu, N. Li, F. Xiao, Microporous Mesoporous Mater. 57 (2003) 191.
[34] T. Kimura, Y. Sugahara, K. Kuroda, Chem. Lett. (1997) 983.

[35] D. Zhao, Z. Luan, L. Kevan, Chem. Commun. (1997) 1009.
[36] M. Tiemann, M. Froba, Chem. Mater. 13 (2001) 3211.
[37] C.T. Kresge, M.E. Leonowicz, W.J. Roth, J.C. Vertuli, J.S. Beck, Nature 359 (1992) 710.
[38] P. Selvam, S.K. Bhatia, C. Sonwane, Ind. Eng. Chem. Res. 40 (2001) 3237.
[39] S.K. Mohapatra, B. Sahoo, W. Keune, P. Selvam, Chem. Commun. (2002) 1466.
[40] R. A Sheldon, J.K. Kochi, Metal-Catalyzed Oxidations of Organic Compounds, Academic Press, New York, 1981.
[41] C.L. Hill, Activation, Functionalization of Alkanes, Wiley, New York, 1989.
[42] R. Raja, G. Sankar, J.M. Thomas, J. Am. Chem. Soc. 121 (1999) 11926.
[43] M. Nowotny, L.N. Pedersen, U. Hanefeld, T. Maschmeyer, Chem. Eur. J. 8 (2002) 3724.
[44] A. Sakthivel, P. Selvam, J. Catal. 211 (2002) 134.
[45] S.K. Mohapatra, P. Selvam, Top. Catal. 22 (2003) 17.
[46] D.H.R. Barton, E. Csuhai, N. Ozbalik, Tetrahedron Lett. 46 (1990) 3743.
[47] U. Schuchardt, D. Mandelli, G.B. Shul'pin, Tetrahedron Lett. 37 (1996) 37.
[48] J.-H. In, S.-E. Park, R. Song, W. Nam, Inorg. Chem. Acta 343 (2003) 373.
[49] S.A. Bagshaw, E. Prouzet, T.J. Pinnavaia, Science 269 (1995) 1242.
[50] R. Ryoo, J.M. Kim, C.H. Ko, J. Phys. Chem. 100 (1996) 17718.
[51] J.M. Bennett, J.P. Cohen, E.M. Flanigen, J.J. Pluth, J.V. Smith, ACS Sym. Ser. 218 (1983) 109.
[52] S.J. Gregg, K.S.W. Sing, Adsorption, Surface Area and Porosity, 2nd ed., Academic Press, London, 1982.
[53] Z. Luan, D. Zhao, H. He, J. Klinowski, L. Kevan, J. Phys. Chem. B 102 (1998) 1250.
[54] J.W. Park, H. Chon, J. Catal. 133 (1992) 159.
[55] D. Goldfab, M. Bernardo, K.G. Strohmaier, D.E.W. Vaughan, H. Thomann, J. Am. Chem. Soc. 116 (1994) 6344.
[56] S. Bordiga, R. Buzzoni, F. Geobaldo, C. Lamberti, E. Giamello, A. Zecchina, G. Leofanti, G. Petrini, G. Tozzola, G. Vlaic, J. Catal. 158 (1996) 486.
[57] P. Fejes, I. Kiricsi, K. Kovács, K. Lázár, I. Marsi, A. Oszkó, A. Rockenbauer, Z. Schay, Appl. Catal. A 223 (2002) 147.
[58] S.E. Dapurkar, S.K. Badamali, P. Selvam, Catal. Today 68 (2001) 63.
[59] S.E. Dapurkar, P. Selvam, Mater. Phys. Mech. 4 (2001) 13.
[60] E.L. Pires, J.C. Magalhaes, U. Schuchardt, Appl. Catal. A 203 (2000) 231.
[61] T.G. Traylor, J.S. Buyn, P.S. Trylor, P. Battoni, D. Mansuy, J. Am. Chem. Soc. 113 (1991) 7821.
[62] A.S. Goldstein, R.H. Beer, R.S. Drago, J. Am. Chem. Soc. 116 (1994) 2424.
[63] N. Mizuno, C. Nozaki, I. Kiyoto, M. Misono, J. Am. Chem. Soc. 120 (1998) 9267.
[64] R.F. Parton, G.J. Peere, P.E. Neys, P.A. Jacobs, R. Claessens, G.V. Baron, J. Mol. Catal. A 113 (1996) 445.
[65] P.A. Mac, I.W. Faul, C.E. Arends, K.U. Ingold, D.D.M. Wayner, J. Chem. Soc., Perkin Trans. 2 (1997) 135.
[66] R.A. Sheldon, Top. Curr. Chem. 164 (1993) 23.
[67] P. Knops-Gerrits, D.D. Vos, F. Thibault-Starzyk, P.A. Jacobs, Nature 369 (1994) 543.
[68] W. Zhang, J. Wang, P.T. Tanev, T.J. Pinnavaia, Chem. Commun. (1996) 979.
[69] S.K. Mohapatra, F. Hussain, P. Selvam, Catal. Commun. 4 (2003) 57.
[70] Ch. Subrahmanyam, B. Viswanathan, T.K. Varadarajan, J. Mol. Catal. A 223 (2004) 149.
[71] R.A. Leising, J. Kim, M.A. Peraz, L. Que Jr., J. Am. Chem. Soc. 115 (1993) 9524.
[72] C. Kim, K. Chen, J. Kim, L. Que Jr., J. Am. Chem. Soc. 119 (1997) 5964.
[73] P. Selvam, S.K. Mohapatra, J. Catal. 233 (2005) 276.